

Synthesis and memory characteristics of highly organo-soluble polyimides bearing a noncoplanar twisted biphenyl unit containing aromatic side-chain groups†

Yueqin Li,^{ab} Huihua Xu,^a Xian Tao,^a Kejia Qian,^b Shuang Fu,^b Yingzhong Shen^{*ab} and Shijin Ding^{*b}

Received 5th August 2010, Accepted 25th October 2010

DOI: 10.1039/c0jm02547j

Two novel 3',4',5'-trifluorobiphenyl-based aromatic polyimide monomers, 2,2'-bis[4'-(3'',4'',5''-trifluorophenyl)phenyl]-4,4'-biphenyl diamine (BTFBPD) and 2,2'-bis[4'-(3'',4'',5''-trifluorophenyl)phenyl]-4,4',5,5'-biphenyltetracarboxylic dianhydride (BTFBPDA) were synthesized. Two fluorinated polyimides (PIs), PI(BTFBPD-DPBPDA) and PI(BTFBPD-BTFBPDA) were prepared *via* a two-step procedure using BTFBPD reacting with 2,2'-diphenyl-4,4',5,5'-biphenyltetracarboxylic dianhydride (DPBPDA) and BTFBPDA, respectively. BTFBPD was characterized with single crystal X-ray diffraction analysis and the geometric parameters showed the noncoplanar twisted character. PIs exhibited highly organo-solubility and thermal stability. The PI films sandwiched between an indium-tin oxide (ITO) bottom electrode and Al top electrode exhibited two accessible conductivity states and can be switched from the low-conductivity to the high-conductivity. The memory devices with the configuration of Al/PI(BTFBPD-DPBPDA)/ITO exhibited a flash type memory capability, whereas the Al/PI(BTFBPD-BTFBPDA)/ITO presented a write once read many times (WORM) memory capability. The fabricated devices showed low turn-on threshold voltages of -1.3 V (PI(BTFBPD-DPBPDA)) and -1.7 V (PI(BTFBPD-BTFBPDA)) and both ON/OFF current ratios on the order of 10^3 to 10^4 .

Introduction

Electrically switching organic molecules and polymeric materials have attracted more and more attention as alternative or supplemental materials to traditional inorganic materials in the application of resistive random access memory (RRAM) in recent years.¹⁻⁴ Polymeric materials not only exhibit low-cost potential, simplicity in structure, good scalability, and potential for high density data storage in 3D arrays but also their properties can be easily tailored through chemical synthesis.⁵ Therefore, there is currently much research into the development of new polymer switching materials with properties and processability that meet the requirements of nonvolatile or volatile memory devices, including conjugated polymers,⁶⁻¹² electron donor/acceptor polymers,^{13,14} polymer nanocomposites embedded metal nanoparticle and fullerene,^{1-3,15} and polymers with specific pendant chromophores.¹⁶⁻²⁰ Rather than encoding "0" and "1" as the amount of charge stored in a cell in silicon devices, polymer memory stores data, for instance, based on the high and low-conductivity response to an applied voltage.²¹ Different kinds of memory devices have been also explored, such as

dynamic random access memory (DRAM), write-once-read-many (WORM) and flash memory, *etc.* The mechanisms responsible for electrical conduction, switching and nonvolatile effects were summarized as carrier trapping-detrapping, electric-field induced charge transfer (CT), filamentary metal, conformational behaviors and phase changes, and redox effects.²²

Among the entire studied polymer systems, electron donor/acceptor polymers, especially functional polyimides have been widely investigated owing to their excellent thermal stability, good processability, and superior mechanical properties besides the electrical switching behavior.²³⁻²⁹ Polyimides containing electron donor and electron acceptor groups exhibit bistable resistive switching arising from field-conducted CT processes, wherein imide groups acted as the electron acceptor. The reported polyimides were poly(3,3'-bis(diphenylcarbamyloxy)-4,4'-biphenylenehexafluoroisopropylidenediphtalimide) (6F-HAB-DPC PI),²³ poly(4,4'-aminotriphenylenehexafluoroisopropylidenediphtalimide) (6F-TPA PI),¹³ poly(3,3'-bis(*N*-ethylenyloxycarbazole)-4,4'-biphenylenehexafluoroisopropylidenediphtalimide) (6F-HAB-CBZ PI),¹⁹ poly(3,3'-di(4-(diphenylamino)benzylidene)liminoethoxy)-4,4'-biphenylenehexafluoroisopropylidenediphtalimide) (6F-HAB-TPAIE PI),²⁴ poly(*N*-(*N'*,*N'*-diphenyl-*N'*-1,4-phenyl)-*N*,*N*-4,4'-diphenylenehexafluoroisopropylidenediphtalimide) (6F-2TPA PI),²⁵ poly(4,4'-amino(4-hydroxyphenyl)-diphenylenehexafluoroisopropylidenediphtalimide) (6F-HTPA PI),²⁶ poly(2,7-bis(phenylenesulfanyl)thianthrenehexafluoroisopropylidenediphtalimide) (APTT-6FDA PI) and poly(4,4'-thiobis(*p*-phenylenesulfanyl)hexafluoroisopropylidenediphtalimide) (3SDA-6FDA PI),²⁷ poly(4-amino-4'-(*p*-aminophenoxy)triphenylaminehexafluoroisopropylidenediphtalimide)triphenylaminehexafluoroisopropylidenediphtalimide) (APT-TPA PI),²⁸

^aApplied Chemistry Department, School of Material Science & Engineering, Nanjing University of Aeronautics & Astronautics, Nanjing, 210016, P. R. China. E-mail: yz_shen@nuaa.edu.cn; Fax: +86-25-52112626; Tel: +86-25-52112906-84765

^bState Key Laboratory of ASIC and System, School of Microelectronics, Fudan University, Shanghai, 200433, P. R. China. E-mail: sjding@fudan.edu.cn; Fax: +86-21-55664845; Tel: +86-21-55664845

† Electronic supplementary information (ESI) available: FT-IR, ¹H-NMR, ¹³C-NMR spectra of BDBPDA and BTFBPDA. CCDC reference numbers 715156, 784374. For ESI and crystallographic data in CIF or other electronic format see DOI: 10.1039/c0jm02547j

poly(2,5-bis(*p*-aminophenoxyphenyl)-1,3,4-oxadiazolehexafluoroisopropylidenediphthalimide) (P(BPPO)-PI).²⁹ The triphenylamino (TPA) moieties as electron donor have been proposed to enhance the electron donating and charge transport ability with phthalimide moieties (electron acceptor). The 6F-TPA PI containing TPA moieties has been reported to exhibit volatile memory (*i.e.*, dynamic random access memory (DRAM)) behavior with bipolar ON- and OFF-switching characteristics.¹³ In contrast, the TPA-PPF PI exhibits WORM behavior in negative voltage sweeps, even though the polymer contains the same TPA moieties. On the other hand, the 6F-2TPA PI, which contains connected two TPA moieties, reveals unipolar WORM characteristic as well as DRAM behavior with polarity, depending on the film thickness.²⁵ The mono- or dual-mediated phenoxy linkages between the TPA and phthalimide moieties, represented as (D-L-A)*n* (PI(AAPT-6FDA)) or (L-D-L-A)*n* (PI(APT-6FDA)), was found to significantly affect the volatile memory behaviors. PI(AAPT-6FDA) exhibited DRAM performance, while PI(APT-6FDA) showed the static random access memory (SRAM) behavior.²⁸ The role of TPA moiety in the electrically bistable characteristics of these polymers remain questionable and these results collectively suggest that the electrical memory behavior of a polyimide is sensitively dependent upon the chemical natures of the constituent parts in the polymer. The development of highly stable memory devices based on dimensionally and thermally stable polymers remains in the exploration stage. Therefore, the relationship between the polymer structure and memory characteristics requires further exploration.

Among various polyimide-based memory devices developed, the 4,4'-hexafluoroisopropylidenediphthalic anhydride (6FDA) moiety played an important role in enhancing the electron acceptor ability of imide group,^{5,13} and it was widely used as the anhydride monomer to synthesize functional polyimides in bistable memory devices. However, 2,2'-position aryl-substituted tetracarboxylic dianhydride and diamine as polyimide monomers have not been explored for such applications. In general, introduction of bulky substituent into 2,2'-position of biphenyl can produce high levels of ring-torsion and induce non-coplanar structure. On one hand, the non-planar twisted biphenyl moieties would push the neighboring chains apart to disrupt the crystal packing and enhance solubility and sustain superior thermal stability and mechanical property.^{30–33} On the other hand, the non-planar configuration of organic data storage materials would suppress intramolecular coupling for the energy barrier induced by the torsion angle.³⁴ Meanwhile, the intermolecular charge transfer would be promoted and charge recombination becomes difficult. Moreover, the noncoplanar configuration will contribute to a large current ratio of ON/OFF because it perturbs conjugation in the molecular backbone and results in a comparatively low conductance state (OFF).³⁴ In this study, we report the synthesis and fabrication of novel programmable “write–read–erase” memory devices based on nano-scale thin films of soluble and thermally stable polyimides, such as PI(BTFBPD-DPBPDA) derived from 2,2'-bis[4'-(3'',4'',5''-trifluorophenyl)phenyl]-4,4'-biphenyl diamine (BTFBPD) reacting with 2,2'-diphenyl-4,4',5,5'-biphenyltetracarboxylic dianhydride (DPBPDA) and PI(BTFBPD-BTFBPDA) from BTFBPD and 2,2'-bis[4'-(3'',4'',5''-trifluorophenyl)phenyl]-4,4',5,5'-biphenyl tetracarboxylic dianhydride (BTFBPDA) (Fig. 1). The 3',4',5'-

trifluorobiphenyl and phenyl moieties as pendants are expected to be the electron donors and phthalimide moieties act as the electron acceptors. The thermal, optical, and electrochemical properties of PI(BTFBPD-DPBPDA) and PI(BTFBPD-BTFBPDA) were also investigated. These PIs exhibit good solubility in common organic solvents so they can be easily fabricated by means of conventional solution spin-coating and subsequent drying. The memory behavior was estimated by a simple sandwich device configuration consisting of polymer films as active layer between ITO ground electrode and Al top electrode. PI(BTFBPD-DPBPDA) exhibited a flash type memory behavior, while PI(BTFBPD-BTFBPDA) presented a WORM memory behavior. Both of them maintained a long retention time in ambient conditions. The electrical characteristics suggested that PI(BTFBPD-DPBPDA) and PI(BTFBPD-BTFBPDA) were expected candidates for organic bistable memory materials.

Experimental

Materials

Phenylboronic acid and 3',4',5'-trifluorobiphenyl-4-ylboronic acid (99%, Hebei Delongtai Chemicals Co., Ltd.) and 3,3',4,4'-biphenyltetracarboxylic dianhydride (BPDA, 99%, Changzhou Wujin Linchuan Chemical Co., Ltd.) were used as received. 2,2'-Dibromobiphenyl-4,4'-diamine was synthesized on the basis of ref. 35. 4,4'-Bis(*N*-methylphthalimide) was prepared according to the literature.³⁰ All the other reagents and solvents were analytical-grade and were used without further purification.

Measurements

The FT-IR measurements (KBr pellets) were recorded in the range of 400–4000 cm⁻¹ on the instrument of Thermo Nicolet Nexus 670 infrared spectrometer. NMR spectra were recorded on a Bruker Advance 300 spectrometer at resonant frequencies of 300 MHz for ¹H and 75 MHz for ¹³C nuclei using CDCl₃ and DMSO-*d*₆ as solvent and tetramethylsilane as the reference. Weight average molecular weight (*M*_w) and number average molecular weight (*M*_n) were determined by gel permeation chromatography (GPC) on a Water GPC system equipped with

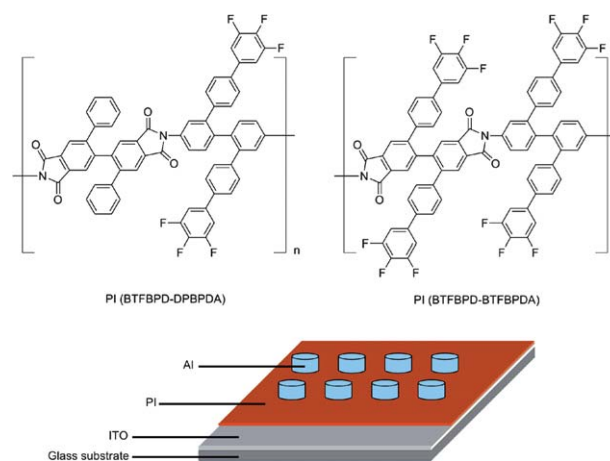


Fig. 1 Molecular structure of PIs and schematic diagram of the memory devices consisting of a thin film of PIs (about 50 nm) sandwiched between an ITO bottom electrode and an Al top electrode.

four Water Ultrastyrigel columns (300 × 7.5 mm, guarded and packed with 1 × 10⁵, 1 × 10⁴, 1 × 10³, and 500 Å gels) in series. Tetrahydrofuran (THF, 1 mL min⁻¹) was used as the eluent. The effluents were monitored by a UV detector (JMST Systems, VUV-24, USA) at the wavelength of 254 nm. Monodispersed polystyrene was used as the molecular weight standard. Elemental analysis was performed on a Perkin-Elmer 240 C elemental analyzer. Thermo Gravimetric Analysis (TGA) and Differential Scanning Calorimetric (DSC) studies were carried out with a NETZSCH STA 449 C with a constant heating rate of 10 °C min⁻¹ under argon flow rate of 1.0 cm³ min⁻¹. X-ray powder diffraction patterns were obtained with a Bruker D8-Advance model X-ray diffractionmeter with a Ni-filter and graphite monochromator, and Cu-Kα1 radiation (λ = 1.54056 Å, 40 kV, 50 mA, 4°/min). The single X-ray structure measurement was performed on a Rigaku SCXmini CCD, detector equipped with graphite monochromatic Mo-Kα radiation (λ = 0.71073 Å) at 297 K. ‡ UV-vis absorption spectra were obtained on a UV-2550 UV-vis spectrophotometer and fluorescence spectra were measured with an Eclipse fluorescence spectrometer. Melting points were measured by WBR-1B melting point digital apparatus. Cyclic voltammogram (CV) was recorded on a CHI 660C electrochemical work station using a glass carbon electrode as the working electrode, Pt plate as the counter electrode, and an Ag/AgCl electrode as the reference. A 0.1 M tetra-*n*-butylammonium perchlorate (*n*-Bu₄ClO₄) in anhydrous acetonitrile was employed as the supporting electrolyte.

Monomer synthesis

2,2'-Bis[4'-(3'',4'',5''-trifluorophenyl)phenyl]-4,4'-biphenyl diamine (BTFBPD). A solution of 2,2'-dibromobiphenyl-4,4'-diamine (3.42 g, 0.01 mol), 4-(3',4',5'-trifluoro)biphenylboronic acid (5.54 g, 0.022 mol), Pd(PPh₃)₄ (0.23 g, 0.2 mmol), Na₂CO₃ (4.24 g, 0.04 mol), in ethanol (40 mL) and water (20 mL) was heated at 80 °C under an nitrogen atmosphere for 4 h. When the reaction was completed, the reaction mixture was cooled and filtered under nitrogen. The filtrate was condensed and extracted twice with 1,2-dichloroethane (2 × 20 mL). The combined organic layer was washed twice with saturated NaHCO₃ solution (40 mL) and water respectively, and then dried over anhydrous MgSO₄. The solvent was evaporated to obtain brown powders. The filter cake and the powders were combined and recrystallized from 1,2-dichloroethane to give a white product (4.5 g, 75%), mp 246 °C (dec.). FT-IR: ν_{max}/cm⁻¹ 3389 and 3433 (N-H), 1363 (C-N), 1041 (C-F). ¹H NMR (300 MHz, δ_H/ppm in DMSO-d₆): δ 7.68 (t, 2 H, ³J_{F-H} = 7.8 Hz, ⁴J_{F-H} = 4.1 Hz), 7.45 (d, 2 H, *J* = 7.95 Hz), 6.91 (d, 1 H, *J* = 8.15 Hz), 6.72 (d, 2 H, *J* = 7.95 Hz), 6.53 (d, 1 H, *J* = 7.9 Hz), 6.37 (s, 1 H), 5.07 (br, 2 H). ¹³C NMR (75 MHz, δ_H/ppm in DMSO-d₆): δ 150.6 (ddd, ¹J_{C-F} = 223.5

Hz, ²J_{C-F} = 9.4 Hz, ³J_{C-F} = 4.1 Hz), 147.4, 142.3, 140.0, 138.1 (dt, ¹J_{C-F} = 231.0 Hz, ²J_{C-F} = 15.7 Hz), 136.4, 133.9, 132.4, 129.3, 127.6, 125.6, 115.0, 113.5, 110.8 (dd, ²J_{C-F} = 15.0 Hz, ³J_{C-F} = 5.6 Hz). Anal. calcd. for C₃₆H₂₂F₆N₂: C, 72.48; H, 3.72; N, 4.70; Found: C, 72.29; H, 3.40; N, 4.68.

4,4'-Bis(2,2'-diiodo-*N*-methylphthalimide) (1). 4,4'-Bis(*N*-methylphthalimide) (51.00 g, 0.16 mol) was added to concentrated H₂SO₄ (98 wt%, 700 mL) in a three-necked round-bottom flask under vigorously stirring. When the solid dissolved completely, KIO₃ (137.00 g, 0.64 mol) and I₂ (81.20 g, 0.32 mol) were added to the mixture, with vigorous stirring for 24 h. After the reaction finished the reaction mixture was poured into ice-water containing the previously dissolved Na₂SO₃ (fume hood). Filtration and the collected precipitate was filtrated and washed thoroughly by water then purified by recrystallization from ethanol to give a white product (73.8 g, 80%). FT-IR: ν_{max}/cm⁻¹ 1775 and 1712(C=O), 1378 (C-N), 1008 (C-I), 741 (imide ring deformation). ¹H NMR (300 MHz, δ_H/ppm in DMSO-d₆): δ 8.46 (s, 1 H), 7.71 (s, 1 H), 3.04 (s, 3 H, CH₃). ¹³C NMR (75 MHz, δ_H/ppm in DMSO-d₆): δ 167.3, 166.3, 132.9, 132.6, 131.8, 123.5, 107.0, 24.0. Anal. calcd. for C₁₈H₁₀I₂N₂O₄: C, 37.79; H, 1.76; N, 4.90; Found: C, 37.72; H, 1.66; N, 4.93.

2,2'-Diiodobiphenyl-4,4',5,5'-tetracarboxylic acid (2). 4,4'-Bis(2,2'-diiodo-*N*-methylphthalimide) (46.38 g, 0.081 mol), KOH (22.68 g, 0.405 mol) dissolved in water (250 mL) was heated to reflux for 24 h, and then made acidic by the addition of 6.5 N HCl to pH of 1.0. The white precipitate was collected by filtration and dried in vacuum at 100 °C to give tetracarboxylic acid (47.00 g, 99%). FT-IR: ν_{max}/cm⁻¹ 3432 (O-H), 1691 and 1293 (C=O), 1086 (C-I). ¹H NMR (300 MHz, δ_H/ppm in DMSO-d₆): δ 8.47 (s, 1 H), 7.71 (s, 1 H). ¹³C NMR (75 MHz, δ_H/ppm in DMSO-d₆): δ 167.4, 166.8, 149.4, 140.6, 134.9, 133.5, 131.5, 102.7. Anal. calcd. for C₁₆H₈I₂O₈: C, 33.02; H, 1.39; Found: C, 33.00; H, 1.41.

Tetraethyl 2,2'-diiodobiphenyl-4,4',5,5'-tetracarboxylate (3). 2,2'-Diiodobiphenyl-4,4',5,5'-tetracarboxylic acid (47.00 g, 0.08 mol), ethanol (20 mL, 0.35 mol), concentrated sulfuric acid (10 mL) and benzene (260 mL) were charged into a 500 mL three-necked flask equipped with a magnetic stirrer, Dean-Stark trap and a reflux condenser. The reaction mixture was heated to 80 °C, and maintained at this temperature for 4 h. The water formed in the reaction was removed by azeotropic benzene. Then the mixture was cooled to room temperature and washed by saturated NaHCO₃, brine, and water, respectively. The organic layer was separated and dried over anhydrous MgSO₄ and concentrated to give yellow residue; it was recrystallized from ethanol to afford white crystals (40.0 g, 72%), mp 94.1–94.6 °C. FT-IR: ν_{max}/cm⁻¹ 1728 (C=O), 1284 and 1135 (C-O-C), 1079 (C-I). ¹H NMR (300 MHz, δ_H/ppm in DMSO-d₆): δ 8.25 (s, 1 H), 7.51 (s, 1 H), 4.32–4.43 (m, 4 H, CH₂), 1.33–1.41 (m, 6 H, CH₃). ¹³C NMR (75 MHz, δ_H/ppm in DMSO-d₆): δ 166.3, 165.9, 149.9, 139.4, 133.7, 131.9, 129.9, 102.2, 62.3, 62.1, 14.2, 14.1. Anal. calcd. for C₂₄H₂₄I₂O₈: C, 41.52; H, 3.48; Found: C, 41.48; H, 3.50.

‡ Crystal structure analysis of BTFBPD. C₃₆H₂₂F₆N₂, *M* = 596.56, crystal system: monoclinic, space group *P*2₁/*c*, *a* = 12.097(8) Å, *b* = 13.934(9) Å, *c* = 16.889(10) Å, α = 90°, β = 94.519(12)°, γ = 90°, *V* = 2838(3) Å³, *T* = 297(2) K, *Z* = 4. *R* (reflections) = 0.0695 (3679), *wR*2 (reflections) = 0.1791 (6471). CCDC reference numbers 715156, 784374. Crystal structure analysis of tetraethyl 2,2'-bis[4'-(3'',4'',5''-trifluorophenyl)phenyl]biphenyl-4,4',5,5'-tetracarboxylate. C₄₈H₃₆F₆O₈, crystal system: monoclinic, space group *P*2₁/*c*, *a* = 17.257(4) Å, *b* = 17.152(3) Å, *c* = 15.542(3) Å, α = 90°, β = 116.36(3)°, γ = 90°, *V* = 4122.0(18) Å³, *T* = 297(2) K, *Z* = 4. *R* (reflections) = 0.0969 (4849), *wR*2 (reflections) = 0.2426 (7489).

Tetraethyl 2,2'-bis[4'-(3'',4'',5''-trifluorophenyl)phenyl]biphenyl-4,4',5,5'-tetracarboxylate (4). A solution of tetraethyl 2,2'-diiodobiphenyl-4,4',5,5'-tetracarboxylate (6.94 g, 0.01 mol), 3',4',5'-trifluorobiphenyl-4-ylboronic acid (5.54 g, 0.022 mol), Pd(PPh₃)₄ (0.23 g, 0.2 mmol) and Na₂CO₃ (4.24 g, 0.04 mol) in toluene (40 mL) and water (20 mL) was heated to 110 °C in an atmosphere of nitrogen for 4 h. When the reaction was completed, the reaction mixture was cooled and filtered. The organic layer was washed with portions of saturated NaHCO₃ solution, brine and water, respectively, and then dried over anhydrous MgSO₄. The solvent was evaporated; the brown residue was recrystallized from ethanol to give a white product (6.2 g, 73%), mp 199–200 °C. FT-IR: $\nu_{\max}/\text{cm}^{-1}$ 1724 (C=O), 1294 and 1137 (C–O–C), 1043 (C–F). ¹H NMR (300 MHz, $\delta_{\text{H}}/\text{ppm}$ in DMSO-*d*₆): δ 7.93 (s, 1 H), 7.52 (s, 1 H), 7.11–7.18 (m, 4 H), 6.60 (d, 2 H, *J* = 8.3 Hz), 4.35–4.48 (m, 4 H, CH₂), 1.35–1.57 (m, 6 H, CH₃). ¹³C NMR (75 MHz, $\delta_{\text{H}}/\text{ppm}$ in DMSO-*d*₆): δ 166.8, 166.7, 151.0 (ddd, ¹*J*_{C–F} = 245.1 Hz, ²*J*_{C–F} = 9.9 Hz, ³*J*_{C–F} = 4.0 Hz), 142.8, 140.7, 138.7 (dt, ¹*J*_{C–F} = 239.7 Hz, ²*J*_{C–F} = 16.2 Hz), 138.4, 136.1, 132.4, 132.3, 129.6, 126.7, 125.6, 111.6 (dd, ²*J*_{C–F} = 15.7 Hz, ³*J*_{C–F} = 5.2 Hz), 62.0, 14.3, 14.2. Anal. calcd. for C₄₈H₃₆F₆O₈: C, 67.45; H, 4.25; Found: C, 67.43; H, 4.53.

2,2'-Bis[4'-(3'',4'',5''-trifluorophenyl)phenyl]-4,4',5,5'-biphenyl-tetracarboxylic dianhydride (BTFBPD) (5). KOH (1.96 g, 5 mmol) was added to a solution of tetraethyl 2,2'-bis[4'-(3'',4'',5''-trifluorophenyl)phenyl]biphenyl-4,4',5,5'-tetracarboxylate (6.00 g, 7 mmol) dissolved in ethanol (100 mL) in a 250 mL of round flask. The reaction mixture was heated to reflux for 24 h. The white precipitate formed was collected by filtration, dissolved in water and acidified by diluted HCl to a pH of 2.0. The light yellow precipitate was collected by filtration and dried under vacuum at 100 °C for 24 h. The above obtained solid was charged in a 100 mL three-necked flask, and a mixture of 20 mL acetic anhydride and 20 mL acetic acid was added. The reaction mixture was gradually heated to 135 °C and maintained at this temperature for 4 h. The yellow precipitate formed was filtered and washed thoroughly by toluene. Dried under vacuum at 110 °C for 24 h and obtained yellow powder (4.70 g, 95%). FT-IR: $\nu_{\max}/\text{cm}^{-1}$ 1845 and 1782 (C=O), 1241 and 1111 (C–O–C), 1041 (C–F). ¹H NMR (300 MHz, $\delta_{\text{H}}/\text{ppm}$ in DMSO-*d*₆): δ 8.43 (s, 1 H), 7.89 (s, 1 H), 7.69 (q, 2 H, ³*J*_{F–H} = 9.4 Hz, ⁴*J*_{F–H} = 6.7 Hz), 7.46 (d, 2 H, *J* = 8.4 Hz), 6.63 (d, 2 H, *J* = 8.4 Hz). ¹³C NMR (75 MHz, $\delta_{\text{H}}/\text{ppm}$ in DMSO-*d*₆): δ 162.7, 162.7, 150.6 (ddd, ¹*J*_{C–F} = 245.0 Hz, ²*J*_{C–F} = 10.3 Hz, ³*J*_{C–F} = 4.4 Hz), 147.3, 145.1, 137.1, 136.8 (dt, ¹*J*_{C–F} = 141.1 Hz, ²*J*_{C–F} = 10.1 Hz), 136.4, 131.6, 130.3, 129.8, 129.4, 128.9, 126.5, 126.3, 111.4 (dd, ²*J*_{C–F} = 14.8 Hz, ³*J*_{C–F} = 6.5 Hz). Anal. calcd. for C₄₀H₁₆F₆O₆: C, 68.00; H, 2.28; Found: C, 68.27; H, 2.16.

2,2'-Diphenyl-4,4', 5,5'-biphenyl tetracarboxylic dianhydride (DPBPDA). 2,2'-Diphenyl-4,4',5,5'-biphenyl tetracarboxylic dianhydride was synthesized by the same method. Tetraethyl 2,2'-diphenyl biphenyl-4,4',5,5'-tetracarboxylate was of 82% yield, mp 160–161 °C. FT-IR: $\nu_{\max}/\text{cm}^{-1}$ 1724 (C=O), 1242 and 1136 (C–O–C). ¹H NMR (300 MHz, $\delta_{\text{H}}/\text{ppm}$ in DMSO-*d*₆): δ 7.84 (s, 1 H), 7.46 (s, 1 H), 7.22 (t, 1 H, *J* = 14.7 Hz), 7.11 (t, 2 H, *J* = 14.9 Hz), 6.56 (d, 2 H, *J* = 8.4 Hz), 4.25–4.34 (m, 4 H, CH₂),

1.25–1.32 (m, 6 H, CH₃). ¹³C NMR (75 MHz, $\delta_{\text{H}}/\text{ppm}$ in DMSO-*d*₆): δ 166.5, 166.2, 143.3, 140.3, 137.9, 132.0, 131.9, 130.3, 129.9, 128.6, 128.0, 127.4, 61.5, 13.9, 13.8. Anal. calcd. for C₃₆H₃₄O₈: C, 72.71; H, 5.76; Found: C, 72.64; H, 5.80. 2,2'-Diphenyl-4,4',5,5'-biphenyl tetracarboxylic dianhydride was of yield 86% and mp 271–272 °C. FT-IR, ¹H NMR and ¹³C NMR data were seen in the supporting information (see Fig. S1†) and in line with that reported in the literature.²⁵

Synthesis of PI(BTFBPD-DPBPDA). 2,2'-Diphenyl-4,4',5,5'-biphenyltetracarboxylic dianhydride (0.4464 g, 1.00 mmol) was added into a solution of BTFBPD (0.5965 g, 1.00 mmol) in dehydrated DMAc (solid content 5 wt%) under nitrogen. The reaction mixture was stirred at ambient temperature for 24 h under a nitrogen atmosphere to form poly(amic acid) (PAA) solution. A mixture of equimolar of acetic anhydride and pyridine was added to the poly(amic acid) solution with stirring at ambient temperature for 1 h, and then the mixture was heated to 100 °C and maintained for 3 h. After being cooled, the viscous polymer solution was poured into methanol. The precipitate was filtered, washed thoroughly with methanol and water, and dried at 100 °C under vacuum for 24 h. Yield: 93%. The number average molecular weight (*Mn*) and weight average molecular weight (*Mw*) values tested by GPC were 24880 and 39820, respectively, with the polydispersity index (PDI = *Mw/Mn*) at 1.6. FT-IR: $\nu_{\max}/\text{cm}^{-1}$ 1778 and 1724 (C=O), 1364 (C–N), 1041 (C–F). Anal. calcd. for (C₆₄H₃₂F₆N₂O₄)_n. Calcd.: C, 76.32; H, 3.21; N, 2.78; Found: C, 76.63; H, 3.57; N, 2.59.

Synthesis of PI(BTFBPD-BTFBPDA). Using BTFBPD as an anhydride, PI(BTFBPD-BTFBPDA) was synthesized by a procedure similar to that of PI(BTFBPD-DPBPDA). The yield of PI(BTFBPD-BTFBPDA) was of 90%. *Mn*, *Mw* and PDI values of PI(BTFBPD-BTFBPDA) were 21660, 30330 and 1.4, respectively. FT-IR: $\nu_{\max}/\text{cm}^{-1}$ 1779 and 1726 (C=O), 1365 (C–N), 1044 (C–F). Anal. calcd. for (C₇₆H₃₄F₁₂N₂O₄)_n. Calcd.: C, 72.02; H, 2.71; N, 2.21; Found: C, 71.79; H, 2.97; N, 2.44.

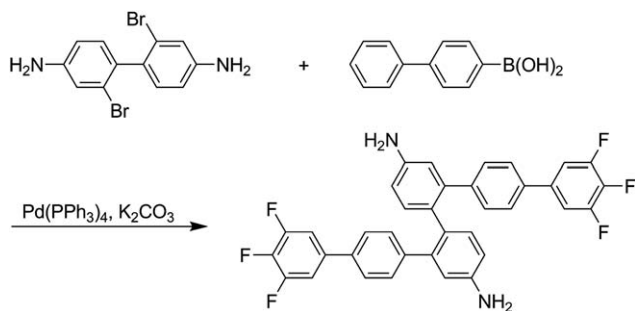
Fabrication and electrical characterization of memory devices.

The indium-tin oxide (ITO, 200 nm in thickness) coated onto glass substrate was used as a bottom electrode. Prior to coating of the polymer film, the ITO surface was cleaned sequentially with deionized water, acetone and isopropanol by sonication for 15 min. Subsequently, a DMAc solution of PI (9 mg mL⁻¹) filtered through polytetrafluoroethylene (PTFE) membrane microfilters with a pore size of 0.22 μm was spin-coated onto the ITO substrate at a rotation rate of 2000 rpm for 60 s, followed by solvent removal in a vacuum at 60 °C for 16 h. The thickness of the polymer layer was about 50 nm, as determined by the Microfigure Measuring Instrument (Surforder ET-3000). Finally, an Al top electrode with an area of 0.0314 mm² and a thickness of about 110 nm was formed by thermal evaporation onto the polymer surface through a shadow mask at a pressure of about 10⁻⁶ Torr. All electrical measurements of the devices were characterized under ambient conditions, without any encapsulation, using a HP 4145B semiconductor analyzer. ITO was maintained as the ground electrode during the electrical measurements and Al was set as the cathode during the voltage sweep.

Results and discussion

Monomer synthesis

In this study, a new functional compound, BTFBPD was successfully synthesized by Suzuki reaction with a high yield of 75% (Scheme 1), which contains 3',4',5'-trifluorobiphenyl moieties. The FT-IR spectrum (Fig. 2) of the obtained compound presents the characteristic absorption of N–H asymmetric stretching and symmetric stretching located at 3443 and 3356 cm^{-1} and the characteristic absorption due to the C–F at 1240 cm^{-1} . ^1H and ^{13}C NMR spectra of BTFBPD are shown in Fig. 3 and Fig. 4, respectively, with the assignment of the observed resonance. For BTFBPD, the proton peaks of aromatic ring appeared at 6.37–7.68 ppm, the coupling constants of $^3J_{\text{F-H}}$ and $^4J_{\text{F-H}}$ were 7.8 and 4.1 Hz, respectively; the carbon peaks of aromatic ring appeared at 110.8–150.6 ppm, the coupling constants of $^1J_{\text{C-F}}$, $^2J_{\text{C-F}}$ and $^3J_{\text{C-F}}$ were 223.5, 9.4 and 4.1 Hz, respectively. All the spectroscopic data were in good agreement with the expected structure. The molecular structure of the diamine was also confirmed by single crystal X-ray diffraction. Single crystal of BTFBPD could be grown by evaporation of saturated 1,2-dichloroethane solution. The molecular structure of BTFBPD was demonstrated in Fig. 5. The dihedral angle of the two central nitrogen-connected phenyl rings (plane 1: C13–C18 and plane 2: C19–C20) was 54.4° . And the dihedral angle between 1,4-disubstituted phenyl ring (plane 3: C7–C12) and the central nitrogen-connected phenyl ring (plane 1) was 50.8° , while a delicate difference dihedral angle



Scheme 1 The synthetic route of BTFBPD.

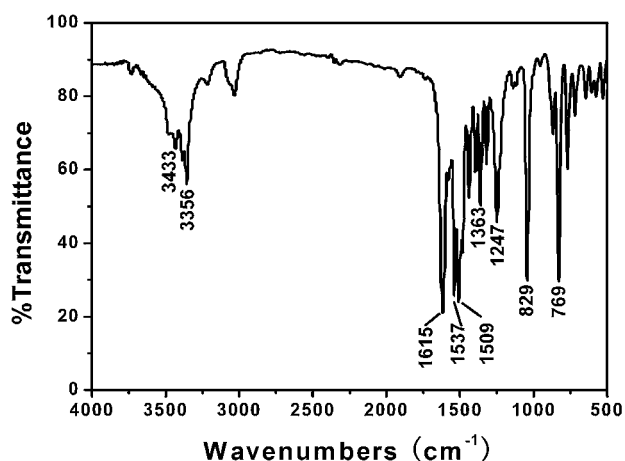


Fig. 2 FT-IR spectrum of BTFBPD.

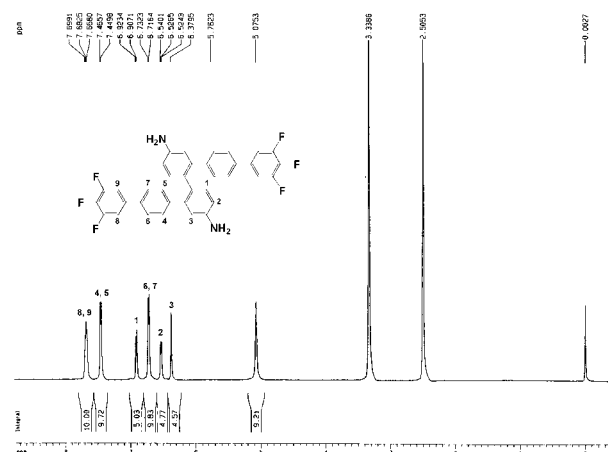


Fig. 3 ^1H NMR spectrum of BTFBPD.

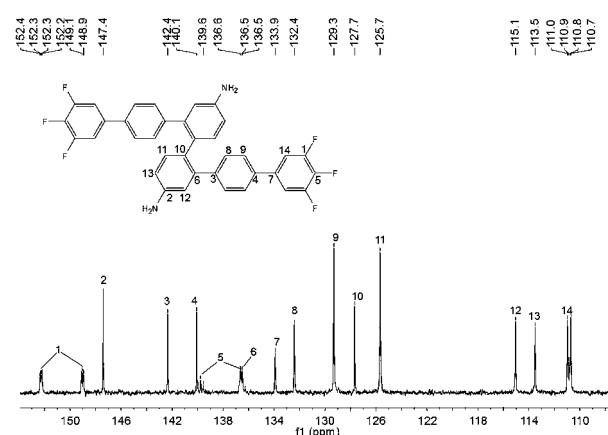


Fig. 4 ^{13}C NMR spectrum of BTFBPD.

between plane 1 and plane 5 (C25–C30) was 48.8° on the other side. Meanwhile, the dihedral angle between plane 3 and plane 4 (C1–C6) was 25.6° , which is smaller than that of plane 5 and plane 6 (C31–C36) 34.6° . Most of all, the dihedral angle between plane 3 and plane 5 was 15.5° , which are close to parallel. As shown in Fig. 5, compound BTFBPD displayed a rod-like

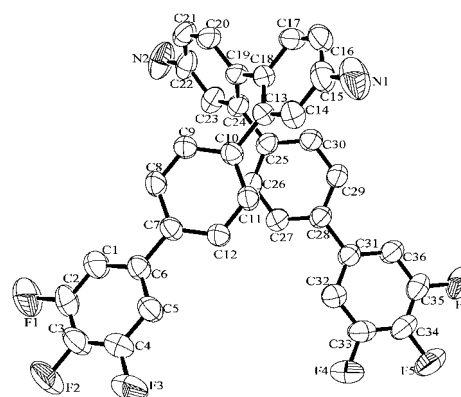
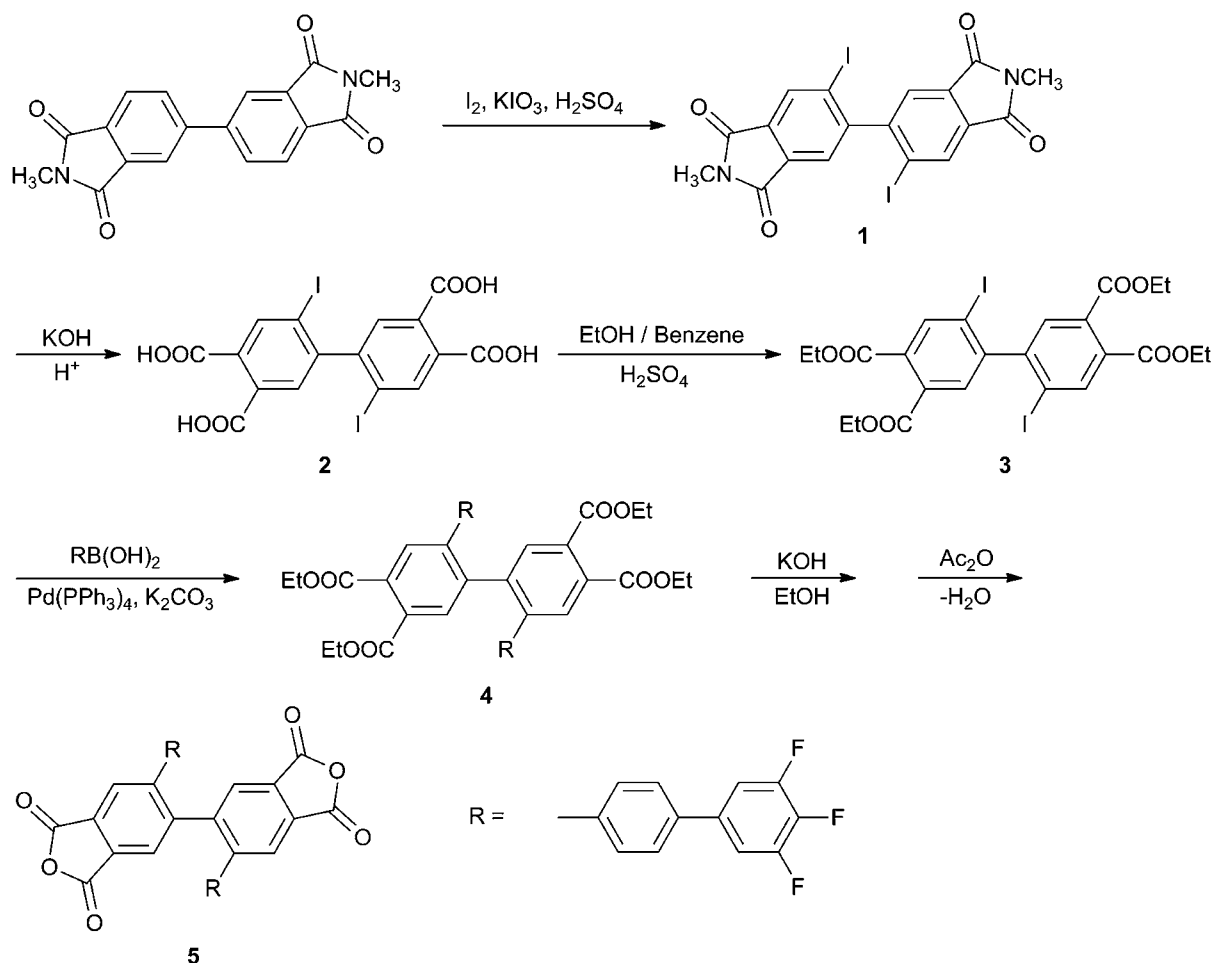


Fig. 5 ORTEP drawing of BTFBPD, showing 30% probability displacement ellipsoids and the hydrogen atoms are omitted for clarity.

twisted geometry configuration. This three-dimensional structure together with the bulky pendant groups in the tetracarboxylic dianhydride will hinder the close packing of polymer chain and enhance the solubility of formed polyimides.

The synthetic route for BTFBPDA tetracarboxylic dianhydride is shown in Scheme 2. The aromatic side-substituted tetracarboxylic dianhydride were synthesized *via* a very important intermediate tetraethyl-2,2'-diiodobiphenyl-4,4',5,5'-tetracarboxylate, which was synthesized from BPDA through four steps. Firstly, BPDA was converted into *N*-methyl imide, and then iodinated by I_2/KIO_3 in concentrated H_2SO_4 under vigorously stirring at room temperature to give 4,4'-bis(2,2'-diiodo-*N*-methylphthalimide). This iodinated imide was ring-opened by KOH and then acidified to form 2,2'-diiodobiphenyl-4,4',5,5'-tetracarboxylic acid, and followed by esterification with ethanol to give tetraethyl-2,2'-diiodobiphenyl-4,4',5,5'-tetracarboxylate. This compound was respectively reacted with phenylboronic acid and 3',4',5'-trifluorobiphenyl-4-ylboronic acid to generate aromatic side-substituted biphenyl tetraethyl tetracarboxylates, and then hydrolyzed by alkali to remove the tetraethyl ester groups and acidified to generate relative biphenyl tetracarboxylic acids. The tetracarboxylic dianhydrides were obtained by dehydration of biphenyl tetracarboxylic acids with acetic anhydride/acetic acid. The yields in each step were high, and the obtained

products in each step were confirmed by FT-IR, 1H NMR, ^{13}C NMR and elemental analysis. Detailed characterization of DPBPDA and BTFBPDA were presented in Fig. S1† and Fig. S2†, respectively. For BTFBPDA, the proton peaks of aromatic ring appeared at 6.63–8.43 ppm, the coupling constants of $^3J_{F-H}$ and $^4J_{F-H}$ were 9.4 and 6.7 Hz, respectively; the carbon peaks of carbonyl group appeared at 162.7 ppm and those of aromatic ring appeared at 110.8–150.6 ppm, the coupling constants of $^1J_{C-F}$, $^2J_{C-F}$ and $^3J_{C-F}$ were 245.0, 10.3 and 4.4 Hz, respectively. In the FT-IR spectrum, the characteristic peak of a carbonyl group of tetracarboxylic dianhydrides appeared at 1787 and 1845 cm^{-1} . The molecular structure of tetraethyl 2,2'-bis[4'-(3'',4'',5''-trifluorophenyl)phenyl]biphenyl-4,4',5,5'-tetracarboxylate was also characterized by single-crystal X-ray diffraction. Single crystal of this compound could be grown by evaporation of saturated 1,2-dichloroethane and ethyl acetate solution. The molecular structure was demonstrated in Fig. 6. The dihedral angle of the two central phenyl rings (plane 1: C4–C12 and plane 2: C28–C36) was 54.58°. And the dihedral angle between 1,4-disubstituted phenyl ring (plane 3: C13–C18) and the central phenyl ring (plane 1) was 53.41°, while a obvious difference dihedral angle between plane 2 and plane 5 (C38–C42) was 42.13° on the other side. Meanwhile, the dihedral angle between plane 3 and plane 4 (C19–C24) was 49.67°, which is



Scheme 2 The synthetic route of BTFBPDA.

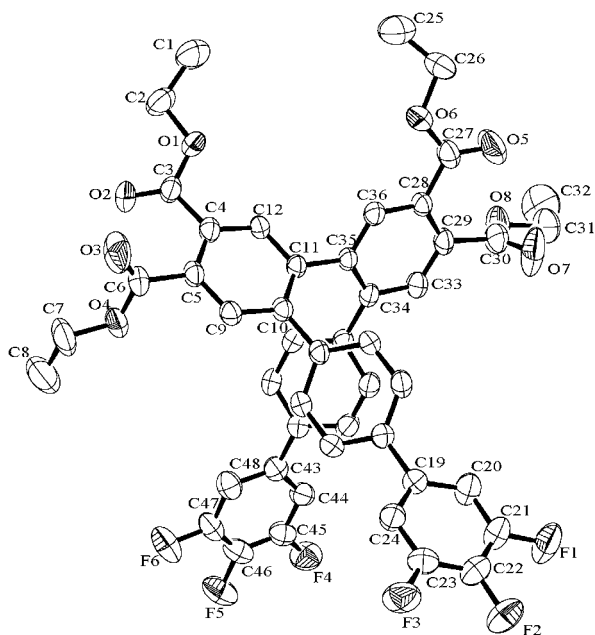


Fig. 6 ORTEP drawing of tetraethyl 2,2'-bis[4'-(3'',4'',5''-trifluorophenyl)phenyl]biphenyl-4,4',5,5'-tetracarboxylate, showing 30% probability displacement ellipsoids and the hydrogen atoms are omitted for clarity.

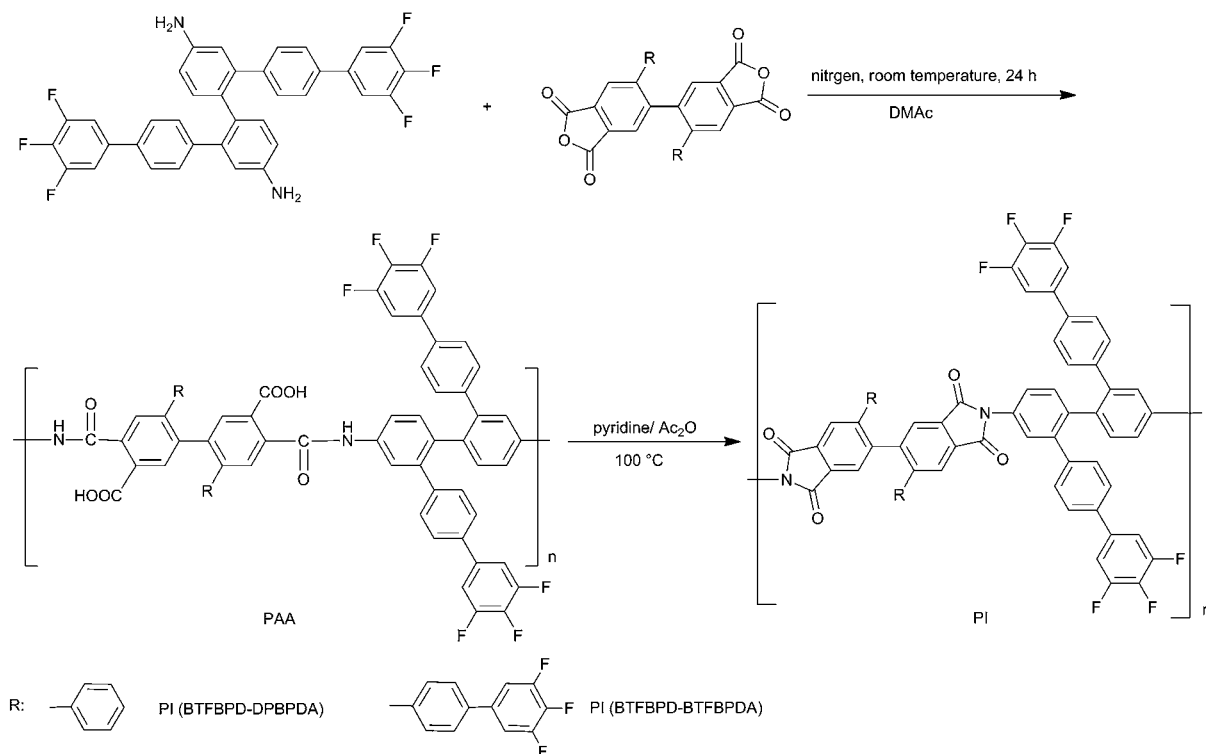
larger than that of plane 5 and plane 6 (C43–C48) 34.6°. Most of all, the dihedral angle between plane 3 and plane 5 was 27.26°. As shown in Fig. 6, this compound also displayed a rod-like twisted geometry configuration.

The polymers, PI(BTFBPD-DPBPDA) and PI(BTFBPD-BTFBPDA) were prepared by the polycondensation of the

diamine (BTFBPD) with tetracarboxylic dianhydrides (DPBPDA and BTFBPDA) in two steps, as shown in Scheme 3. First, diamine and tetracarboxylic dianhydride was dissolved in *N,N*-dimethylacetamide (DMAc) (solid content 5 wt%) under nitrogen to yield a viscous PAA solution. Then, chemical imidization was carried out by adding equimolar of acetic anhydride and pyridine into the PAA solution to produce the polyimide. The two PIs were characterized by the FT-IR spectra (Fig. 7), which shown the typical absorption peaks of the imide moiety at about 1780 cm^{-1} (asymmetrical stretching of C=O), 1720 cm^{-1} (symmetrical stretching of C=O), the C–N bond at about 1360 cm^{-1} and the imide ring deformation at about 740 cm^{-1} . In addition, the characteristic absorption of the C–F group located at about 1040 cm^{-1} can also be observed. In the case of polymers with amide linkages in the main chain, the FT-IR spectra are not sufficient to confirm the complete imidization. Full imidization in poly(amide imides) was confirmed by elemental analysis.

Polymer properties

Organo-solubility and thermal properties of polymers. The solubility properties of the polyimides in several common organic solvents at 10% (w/v) are also presented in Table 1. These polymers exhibited good solubility in a variety of polar solvent such as DMAc, *N,N*-dimethylformamide (DMF), *N*-methylpyrrolidone (NMP), and THF at room temperature or upon heating at 80 °C; however, they were slightly soluble or insoluble in less polar solvent like CHCl_3 , acetone and toluene. Furthermore, the intrinsic viscosities of PI(BTFBPD-DPBPDA) and PI(BTFBPD-BTFBPDA) were of 0.78 and 0.64 dL g^{-1} , respectively. The high solubility may be attributed to the introduction of bulky side-chain substituted groups in the polymer structure.



Scheme 3 Synthesis of PI(BTFBPD-DPBPDA) and PI(BTFBPD-BTFBPDA).

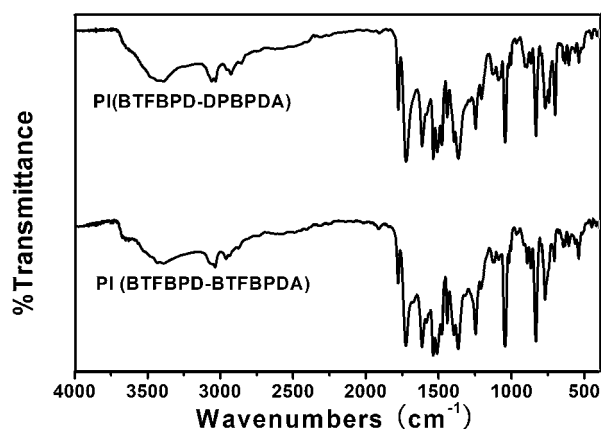


Fig. 7 FT-IR spectra of PI(BTFBPD-DPBPDA) and PI(BTFBPD-BTFBPDA).

The PIs were characterized with X-ray powder diffraction studies. From the diffraction pattern (Fig. S3†), it was observed that PIs displayed a nearly completely amorphous pattern and failed to show any crystallinity. Apparently the amorphous nature of these aromatic-substituted biphenyl-based polyimides was reflected also in their good solubility. This property provides good quality thin film by means of a conventional solution spin-casting process. The thermal properties of the PIs were investigated by TGA (Fig. 8) and DSC (Fig. S4†). The 5% weight-lost temperature (T_d 5%) of PI(BTFBPD-DPBPDA) and PI(BTFBPD-BTFBPDA) were 556 °C and 548 °C, respectively. These polymers afforded high anaerobic char yield of around 70% at 800 °C in a argon atmosphere. From the DSC curves, no Tg signals of the polymers were detected. These results confirm that the new PIs are dimensionally and thermally stable polymers, which meet the requirement of heat resistance in the electronics industry.

Optical and electrochemical properties. The spectra and fluorescence of the studied polymers in THF solution and thin film state were shown in Fig. 9. The concentrations of the polymers for the UV-vis absorption test were about 10^{-6} mol L⁻¹. PI(BTFBPD-DPBPDA) shows the absorption peak maxima (λ_{max}) at 273 and 269 nm in solution and thin film state, while those of PI(BTFBPD-BTFBPDA) were at 276 and 278 nm, respectively. These were assignable to the π - π^* transition, which was attributed to the twisted structure between side chain phenyl or biphenyl and the main chain biphenyl aromatic rings. When these PIs of about 10^{-7} mol L⁻¹ were excited at the maximum absorption wavelength, the emission peaks of PI(BTFBPD-DPBPDA) and PI(BTFBPD-BTFBPDA) were observed at 416

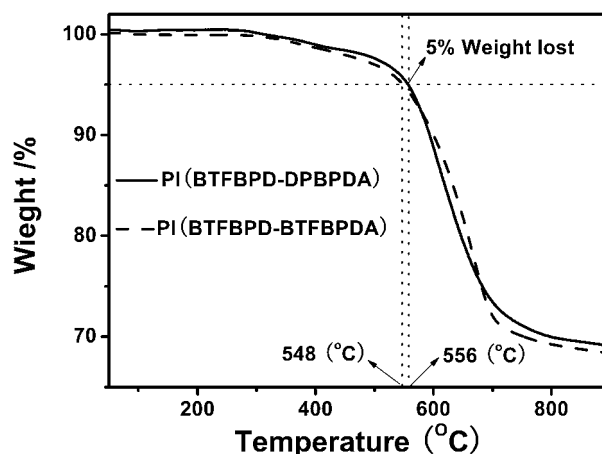


Fig. 8 TGA and DSC curves of PI(BTFBPD-DPBPDA) and PI(BTFBPD-BTFBPDA) under argon atmosphere at a heating rate of 10 °C min⁻¹.

and 426 nm, respectively. The higher fluorescence intensity of PI(BTFBPD-BTFBPDA) compared to PI(BTFBPD-DPBPDA) could be attributed to the incorporation of 3',4',5'-trifluorobiphenyl chromophore. In addition, from Fig. 9, the optical band gap (*i.e.*, the difference between the highest occupied molecular orbital (HOMO) level and the lowest unoccupied molecular orbital (LUMO) level) of PI(BTFBPD-DPBPDA) and PI(BTFBPD-BTFBPDA) from the absorption edges of polymer films are estimated to be 3.66 eV and 3.40 eV, respectively. Therefore, the smaller optical band gap of PI(BTFBPD-BTFBPDA) than that of PI(BTFBPD-DPBPDA) might result from the more twisted configuration by introducing one more 3,4,5-trifluorophenyl moiety. The cyclic voltammetry curves of PI(BTFBPD-DPBPDA) and PI(BTFBPD-BTFBPDA) are shown in Fig. 9, with the PI films coated on a glass carbon electrode in anhydrous acetonitrile containing 0.1 M tetrabutylammonium perchlorate as supporting electrolyte. The oxidation halfwave potential ($E_{1/2}$) for PI(BTFBPD-DPBPDA) and PI(BTFBPD-BTFBPDA) were determined to be 1.67 V and 1.50 V vs. Ag/AgCl, respectively. The external ferrocene/ferrocenium (Fc/Fc⁺) redox standard potential, $E_{1/2}$, was measured to be 0.53 V vs. Ag/AgCl in acetonitrile. Assuming that the HOMO level for the Fc/Fc⁺ standard is -4.80 eV with respect to the zero vacuum level, the HOMO levels for the PI(BTFBPD-DPBPDA) and PI(BTFBPD-BTFBPDA) are determined to be -5.94 eV and -5.77 eV, respectively. Therefore, the LUMO levels of the PI(BTFBPD-DPBPDA) and PI(BTFBPD-BTFBPDA) are estimated to be -2.28 eV and -2.37 eV, respectively. The results suggest that PI(BTFBPD-DPBPDA) could provide a lower and

Table 1 Inherent viscosity and volatility behavior of polymers

Polymer	η_{inh} (dL g ⁻¹) ^a	DMAc	DMSO	DMF	NMP	THF	CHCl ₃	Acetone	Toluene
PI(BTFBPD-DPBPDA)	0.78	<i>b</i>	<i>c</i>	<i>c</i>	<i>c</i>	<i>c</i>	<i>e</i>	<i>e</i>	<i>e</i>
PI(BTFBPD-BTFBPDA)	0.64	<i>b</i>	<i>b</i>	<i>b</i>	<i>b</i>	<i>c</i>	<i>d</i>	<i>e</i>	<i>e</i>

^a inherent viscosity measured at a concentration of 0.5 g dL⁻¹ in DMAc at 30 °C. ^b : soluble at room temperature. ^c : soluble on heating 80 °C. ^d : slightly soluble on heating 80 °C. ^e : insoluble even on heating.

more stable HOMO energy level. The additional twisted side-groups in PI(BTFBPD-BTFBPDA) increased the LUMO energy level slightly, probably due to the nonlinear or twisted conformation of the polymer. In the Al/PI(BTFBPD-DPBPDA)/ITO device, the energy barrier to hole injection from the electrode to the active layer was estimated to be 0.74 eV from the work function (Φ) of ITO (-5.20 eV) and the HOMO of the active PI layer, and the energy barrier to electron injection from the electrode to the active layer was estimated to be 1.92 eV from the Φ of Al (-4.20 eV) and the LUMO of the active layer. This indicates that hole injection from ITO into the HOMO of PI(BTFBPD-DPBPDA) is easier than electron injection from Al into the LUMO of PI(BTFBPD-DPBPDA). Therefore, the PI(BTFBPD-DPBPDA) is a p-type material and holes predominate the conduction process. In the Al/PI(BTFBPD-BTFBPDA)/ITO device, the energy barrier to hole injection from the electrode to the active layer was estimated to be 0.57 eV and the energy barrier to electron injection from the electrode to the active layer was estimated to be 1.83 eV, indicating that the PI(BTFBPD-BTFBPDA) also a p-type material and the conduction process in the device is dominated by hole injection as well.

Electrical characteristics of the PI-based memory devices. The memory effect of PI(BTFBPD-DPBPDA) and PI(BTFBPD-BTFBPDA) was revealed by the current–voltage (I – V) measurements of an Al/polymer/ITO structure. Fig. 10a presents the typical I – V curves of the memory devices fabricated with PI(BTFBPD-DPBPDA). During voltage sweeping from 0 to -4.0 V, the resulting current exhibits a sharp increase by two orders of magnitude at -1.3 V. This indicates that the device is switched from a low conductivity state (OFF state or “0” signal in data storage) to a high conductivity state (ON-state, “1” signal in data storage), which is equivalent to a “writing” process in a digital memory cell. When the voltage is swept backward from -4.0 V to 0 V, the device still remains in a high conductivity state. Further, as the applied voltage is swept from zero to a positive bias, the device is still in a high conductivity state in the initial stage (*i.e.*, corresponding to a larger current). However, the resultant current decreases abruptly by two orders of magnitude when the voltage is increased up to $+4.0$ V. This indicates that the device is restored to an original low conductivity state, which corresponds to the “erasing” process for the memory device.

Moreover, this type of low conductivity state can be maintained during the subsequent positive sweep (see sweep 4) and after the power is turned off. Further, the retention characteristics of the ON/OFF states for the Al/PI(BTFBPD-DPBPDA)/ITO memory cell are shown in Fig. 10b. It is found that the memory cell exhibits two stable states of ON and OFF within 200 min, and the resulting ON/OFF ratio is as large as $\sim 10^3$ under -1.0 V. No degradation was observed during the test.

The electrical behavior of the Al/PI(BTFBPD-BTFBPDA)/ITO device was also investigated as shown in Fig. 10c. During voltage sweeping from 0 to -4.0 V, the current exhibits a sharp increase at around -1.7 V, *i.e.*, from 10^{-6} A to 10^{-2} A. This indicates that the device is switched from a low conductivity state (OFF state) to a high conductivity state (ON state), which serves as the “writing” process for the memory device. After the transition, the device is still in the ON-state even after bias interruption (*i.e.*, 1 min), as revealed by sweep 2. Interestingly, it is observed that the device could not be switched to the low-conductivity state during voltage sweeping from 0 to $+6$ V, as indicated by sweep 3. The storage cells in device show high repeatable I – V characteristics (sweep 4, sweep 5 and sweep 6). The behavior of this memory device which could not be returned to the OFF state by turning off the power and application of a reverse bias exhibits that it is characteristic of a WORM memory device. Further, it is found that an ON/OFF current ratio as high as $\sim 10^4$ is achieved under a constant stress of -1.0 V, and also exhibits superior stability, as displayed in Fig. 10d.

Further information about the charge transport mechanism can be obtained from the I – V curves in OFF and ON states according to various conduction models reported in the literature.^{36–39} As shown in Fig. 11, the OFF states for the Al/PI(BTFBPD-DPBPDA)/ITO device exhibits space charge limited current (SCLC, voltage from 0 to -1.3 V), which can be modeled by the equation as follow:⁴⁰ $I = 9A\epsilon\epsilon_0\mu V^2/8d^3$, where $\epsilon\epsilon_0$ is the absolute permittivity of PI(BTFBPD-DPBPDA), d is the thickness of the polymer film, and μ is the carriers mobility. However, that for the Al/PI(BTFBPD-BTFBPDA)/ITO in the OFF state can be elucidated as Poole–Frenkel (PF)⁴¹ emission in terms of the plots of $\log(I/V)$ vs. $V^{1/2}$ found to be linear in the voltage range of -0.25 to -1.6 V. On the other hand, the currents in the ON state of both devices are almost linear in dependence on applied voltage just as in metallic conduction (Fig. 11b,d); this indicates that in the ON state the charge transport is dominated

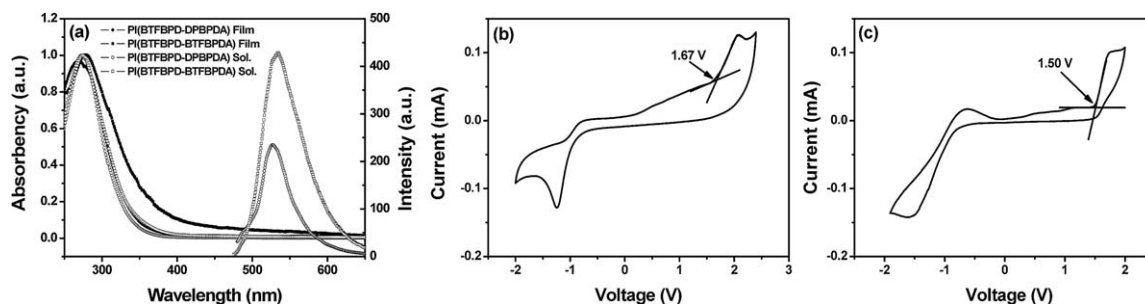


Fig. 9 (a) UV-vis and photoluminescence spectra of PI(BTFBPD-DPBPDA) and PI(BTFBPD-BTFBPDA) in THF solution and thin film state. (b) Cyclic voltammograms of PI(BTFBPD-DPBPDA). (c) Cyclic voltammograms of PI(BTFBPD-BTFBPDA). PI films were coated on a glass carbon electrode in acetonitrile containing 0.1 M tetrabutylammonium perchlorate with a Ag/AgCl (3.8 M KCl) reference electrode and a platinum plate counter electrode. A scan rate of 50 mV s^{-1} was used.

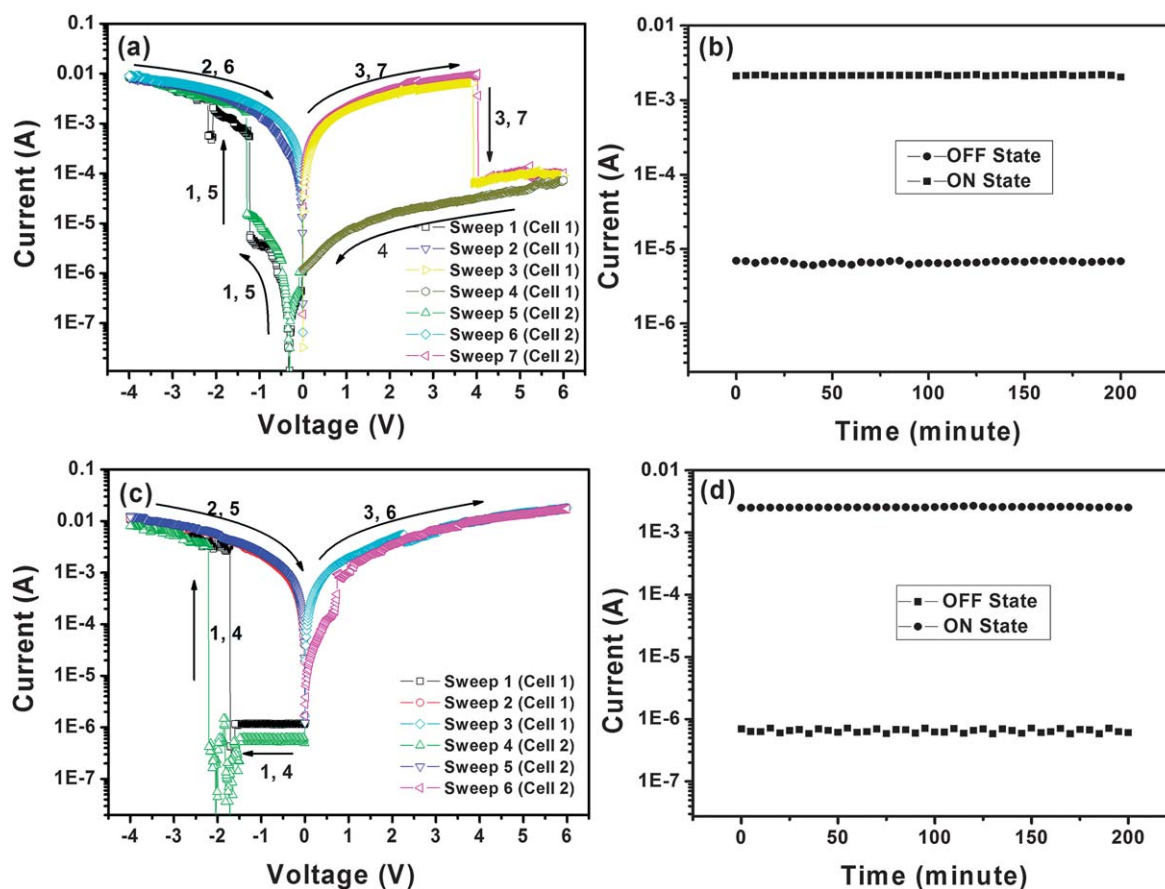


Fig. 10 (a) Current–voltage (I – V) characteristics of a Al/PI(BTFBPD-DPBPDA)/ITO device with an electrode area of 0.0314 mm^2 . (b) Retention characteristics of both ON and OFF states for the Al/PI(BTFBPD-DPBPDA)/ITO device under a constant stress (-1.0 V) at room temperature. (c) Current–voltage (I – V) characteristics of a Al/PI(BTFBPD-BTFBPDA)/ITO device with a electrode area of 0.0314 mm^2 . (d) Retention characteristics of both ON and OFF states for the Al/PI(BTFBPD-BTFBPDA)/ITO device under a constant stress (-1.0 V) at room temperature.

by the ohmic model. Moreover, the current level of our devices in the ON state was found not to be dependent on the device cell size (data not shown), which is indicative of heterogeneously local filament formation.

The above results suggest that the unipolar and bipolar ON and OFF switching behaviors of PI films can be fitted pretty well according to proper theoretical model. Surprisingly, the programmable, digital unipolar and bipolar bistable memory behaviors of PI(BTFBPD-DPBPDA) and PI(BTFBPD-BTFBPDA) in our study are quite different from the DRAM and WORM characteristics of PIs which contain the trifluoromethyl groups and triphenylamino moieties, such as 6F-TPA PI,¹³ 6F-HAB-TPAIE PI,²⁴ and 6F-2TPA PI.²⁵ These interesting bistable memory behaviors may be attributed to differences between the chemical environments of the hole and electron trapping sites in the polymers. The trapping sites might arise due to the chemical composition of the PIs chain, which have different type aryl pendants and two imide rings per unit of the backbone. The aryl pendants are electron donors and thus probably act as nucleophilic sites, whereas imide rings are electron acceptors and probably act as electrophilic sites, so that all repeat units have electric polarization characteristics. Thus, all these groups are likely to act as charge-trapping sites, depending on their associations. As discussed above, for the PIs in this study the energy

barrier for hole injection is lower than that for electron injection, so the conduction process in devices are dominated by hole injection. Thus the pendant units might act as hole-trapping sites, which would explain the observed memory behavior of the PIs-based devices. The pendant units in the PI films are enriched with holes when a bias is applied. At the same time, the imide rings in the PI films are enriched with electrons. When the applied bias reaches the threshold voltage, the trapped charges are able to move through the trapped sites by means of a hopping process (*i.e.* through filament formation), which results in current flow between the bottom and top electrodes. However, switching behaviour of PI(BTFBPD-DPBPDA) and PI(BTFBPD-BTFBPDA) are different. The reason why the device with PI(BTFBPD-DPBPDA) film exhibits excellent flash memory features, whereas that with PI(BTFBPD-BTFBPDA) film exhibits very stable WORM memory behaviors, may be attributed to the difference in the fluorine atom population per unit volume and the different tensional angles between the phenyl rings in the tetracarboxylic dianhydride moiety. Firstly, considering the chemical structures, the population of fluorine atom, which can be able to withdraw electrons and at the same time be holder for holes, is quite different in the polymers. The highly electronegative nature of the fluorine substituent draws electron density from the aromatic π -system, rendering it electron-deficient

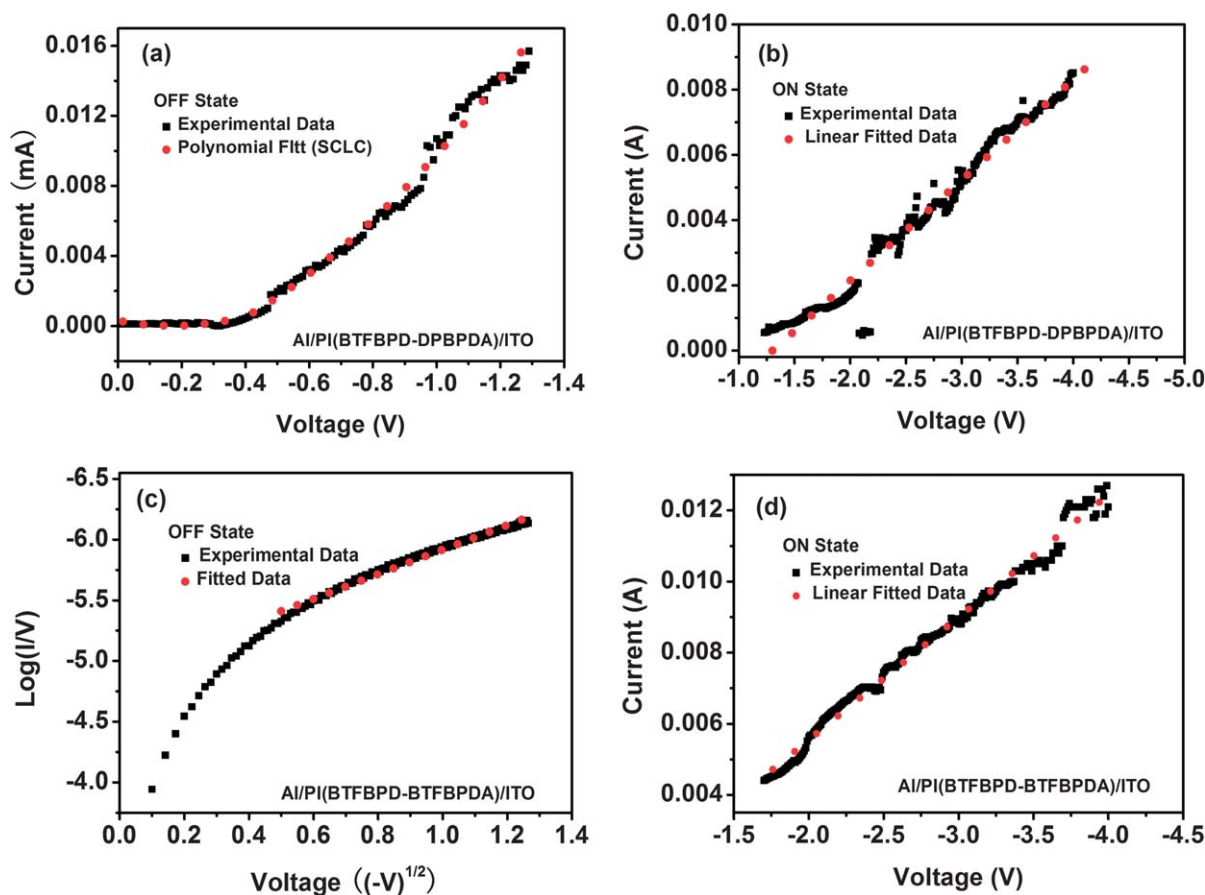


Fig. 11 Experimental and fitted data of I - V curves for the memory devices in the OFF and ON states. Panels (a) and (b) are the OFF state with the SCLC model and the ON state with the ohmic current model for the Al/PI(BTFBPD-DPBPDA)/ITO device. Panels (c) and (d) are the OFF state with the Poole-Frenkel model (-0.25 to -1.6 V) and the ON state with the ohmic current model for the Al/PI(BTFBPD-BTFBPDA)/ITO device.

and more suitable for electron accepting and transporting applications.^{42–45} In particular, the introduction of electron-withdrawing substituents such as fluorine atoms is expected to lower the LUMO level in polyconjugated systems facilitating the electron injection.⁴⁶ So, the difference in the fluorine atom population per unit volume may be strongly related to the observed memory behaviors. Secondly, PI(BTFBPD-BTFBPDA) have two more 3,4,5-trifluorophenyl moieties in the repeat units than PI(BTFBPD-DPBPDA). From the single X-ray analysis of tetraethyl 2,2'-bis[4'-(3'',4'',5''-trifluorophenyl)phenyl]biphenyl-4,4',5,5'-tetracarboxylate, the dihedral angles between the 3',4',5'-trifluorophenyl ring and the 1,4-substituted phenyl ring were up to 49.67°, which may cause more torsional conformation in the PI(BTFBPD-BTFBPDA) backbone. The torsional conformation at the excited state reduces the effective conjugation of the π electrons between neighboring aromatic moieties, and generate an intramolecular potential barrier which prevents the back transfer of charges. In a ring-containing organic molecule, the torsional angle between two aromatic moieties will increase under a static electric field, resulting in an enhanced potential energy barrier for the intramolecular CT and possibly prevent the recombination of segregated charges.⁴⁷ This electrical switching under the applied negative and positive threshold voltage is suggested to form a stable environment temporarily and store the transferred charges. It can prevent the charge from

going back to the initial state even after the application of reverse bias.^{34,47} As a result, the PI(BTFBPD-DPBPDA) could relax to the initial conformation after the removal of the applied electric field for a short period of time. The dihedral angles between the ring moieties reduce to the original state, and also, the potential barriers of back CT disappear. Hence, the back CT occurs from the phthalimide to the pendants (reset to the OFF state) and confirms the volatile switching behavior. Contrarily, the conductive CT state (ON state) of PI(BTFBPD-DPBPDA) is sustained, and cannot be dissociated by a reverse bias without the accompanied conformation relaxation and thus exhibits the WORM switching behavior. Moreover, the more torsional conformation contributes to a comparatively low conductance state (OFF) and results in a larger current ratio of ON/OFF.

Conclusions

In summary, we have synthesized and characterized a novel 2,2'-position aryl substituted diamine (BTFBPD) and anhydrides (DPBPDA and BTFBPDA). Furthermore, these monomers were used for the first time to synthesize two new polyimides, PI(BTFBPD-DPBPDA) and PI(BTFBPD-BTFBPDA), which not only exhibit good organosolubility, high thermal and dimensional stability, but also present electric bistable memory characteristics when using the polyimides as an active layer in

memory devices. The fabricated Al/PI(BTFBPD-DPBPA)/ITO devices have demonstrated a flash type memory behavior with the “write” and “erase” voltages of about -1.3 V and 4.0 V, respectively. Whereas the Al/PI(BTFBPD-BTFBPDA)/ITO devices exhibited a WORM type memory behavior with the “write” voltage of around -1.7 V. In addition, the ON/OFF current ratios of 10^3 – 10^4 are observed in both memory devices. The I – V curves in the OFF and ON state were fitted according to various theoretical models, and it was found that the charge transport in the OFF state was governed by the SCLC model when the active layer was PI(BTFBPD-DPBPA) film and the PF model when the active layer was PI(BTFBPD-BTFBPDA) film, while those in the ON state were both governed by ohmic model. We envision these thermally, dimensionally stable PI(BTFBPD-DPBPA) and PI(BTFBPD-BTFBPDA) polymers are promising materials for mass production at low cost for high-performance, programmable, nonvolatile memory devices that can be operated with low power consumption in unipolar and bipolar switching modes.

Acknowledgements

We are grateful to the financial support from State Key Laboratory of ASIC & System, Fudan University (09KF001).

Notes and references

- 1 S. Möller, C. Perlov, W. Jackson, C. Taussig and S. R. Forrest, *Nature*, 2003, **426**, 166–169.
- 2 J. Y. Ouyang, C. W. Chu, C. R. Szmanda, L. P. Ma and Y. Yang, *Nat. Mater.*, 2004, **3**, 918–922.
- 3 C. W. Chu, J. Quyang, J. H. Tseng and Y. Yang, *Adv. Mater.*, 2005, **17**, 1440–1443.
- 4 Y. Yang, J. Y. Ouyang, L. P. Ma, R. J. Tseng and C. W. Chu, *Adv. Funct. Mater.*, 2006, **16**, 1001–1014.
- 5 Q. D. Ling, D. J. Liaw, E. Y. H. Teo, C. Zhu, D. S. H. Chan, E. T. Kang and K. G. Neoh, *Polymer*, 2007, **48**, 5182–5201.
- 6 T. W. Kim, S. H. Oh, H. Choi, G. Wang, H. Hwang, D. Y. Kim and T. Lee, *Appl. Phys. Lett.*, 2008, **92**, 253308–253308–3.
- 7 T. J. Lee, S. Park, S. G. Hahm, D. M. Kim, K. Kim, J. Kim, W. Kwon, Y. Kim, T. Chang and M. Ree, *J. Phys. Chem. C*, 2009, **113**, 3855–3861.
- 8 S. Park, T. J. Lee, D. M. Kim, J. C. Kim, K. Kim, W. Kwon, Y.-G. Ko, H. Choi, T. Chang and M. Ree, *J. Phys. Chem. B*, 2010, **114**, 10294–10301.
- 9 S. Baek, D. Lee, J. Kim, S. Hong, O. Kim and M. Ree, *Adv. Funct. Mater.*, 2007, **17**, 2637–2644.
- 10 J. Kim, S. Cho, S. Choi, S. Baek, D. Lee, O. Kim, S.-M. Park and M. Ree, *Langmuir*, 2007, **23**, 9024–9030.
- 11 D. Lee, S. Baek, M. Ree and O. Kim, *IEEE Electron Device Lett.*, 2008, **29**, 694–697.
- 12 D. Lee, S. Baek, M. Ree and O. Kim, *Jpn. J. Appl. Phys.*, 2008, **47**, 5665–5667.
- 13 Q. D. Ling, F. C. Chang, Y. Song, C. X. Zhu, D. J. Liaw, D. S. H. Chan, E. T. Kang and K. G. Neoh, *J. Am. Chem. Soc.*, 2006, **128**, 8732–8733.
- 14 S. G. Hahm, S. Choi, S. H. Hong, T. J. Lee, S. Park, D. M. Kim, W. S. Kwon, K. Kim and M. Ree, *Adv. Funct. Mater.*, 2008, **18**, 3276–3282.
- 15 R. J. Tseng, J. X. Huang, J. Ouyang, R. B. Kaner and Y. Yang, *Nano Lett.*, 2005, **5**, 1077–1080.
- 16 A. Kanwal and M. Chhowalla, *Appl. Phys. Lett.*, 2006, **89**, 203103–203103–3.
- 17 Q. D. Ling, S. L. Lim, Y. Song, C. X. Zhu, D. S. H. Chan, E. T. Kang and K. G. Neoh, *Langmuir*, 2007, **23**, 312–319.
- 18 S. L. Lim, N. J. Li, J. M. Lu, Q. D. Ling, C. X. Zhu, E. T. Kang and K. G. Neoh, *ACS Appl. Mater. Interfaces*, 2009, **1**, 60–71.
- 19 C. L. Liu, J. C. Hsu, W. C. Chen, K. Sugiyama and C. Hirao, *ACS Appl. Mater. Interfaces*, 2009, **1**, 1974–1979.
- 20 H. Li, N. J. Li, H. G. Gu, Q. F. Xu, J. M. Lu, X. W. Xia, J. F. Ge and L. H. Wang, *J. Phys. Chem. C*, 2010, **114**, 6117–6122.
- 21 A. Stikeman, *Technol. Rev.*, 2002, **105**, 31.
- 22 Q. D. Ling, D. J. Liaw, C. X. Zhu, D. S. H. Chan, E. T. Kang and K. G. Neoh, *Prog. Polym. Sci.*, 2008, **33**, 917–978.
- 23 S. G. Hahm, S. Choi, S. H. Hong, T. J. Lee, S. Park, D. M. Kim, J. C. Kim, W. Kwon, K. Kim, M. J. Kim, O. Kim and M. Ree, *J. Mater. Chem.*, 2009, **19**, 2207–2214.
- 24 K. Kim, S. Park, S. G. Hahm, T. J. Lee, D. M. Kim, J. C. Kim, W. Kwon, Y. G. Ko and M. Ree, *J. Phys. Chem. B*, 2009, **113**, 9143–9150.
- 25 T. J. Lee, C. W. Chang, S. G. Hahm, K. Kim, S. Park, D. M. Kim, J. Kim, W. S. Kwon, G. S. Liou and M. Ree, *Nanotechnology*, 2009, **20**, 135204–135204–7.
- 26 D. M. Kim, S. Park, T. J. Lee, S. G. Hahm, K. J. Kim, C. Kim, W. S. Kwon and M. Ree, *Langmuir*, 2009, **25**, 11713–11719.
- 27 N. H. You, C. C. Chueh, C. L. Liu, M. Ueda and W. C. Chen, *Macromolecules*, 2009, **42**, 4456–4463.
- 28 T. Kuorosawa, C. C. Chueh, C. L. Liu, T. Higashihara, M. Ueda and W. C. Chen, *Macromolecules*, 2010, **43**, 1236–1244.
- 29 Y. L. Liu, K. L. Wang, G. S. Huang, C. X. Zhu, E. S. Tok, K. G. Neoh and E. T. Kang, *Chem. Mater.*, 2009, **21**, 3391–3399.
- 30 Z. M. Qiu and S. B. Zhang, *Polymer*, 2005, **46**, 1693–1700.
- 31 F. W. Harris, S. H. Lin, F. M. Li and S. Z. D. Cheng, *Polymer*, 1996, **37**, 5049–5057.
- 32 Y. H. Kim, H. S. Kim, S. K. Ahn, S. O. Jung and S. K. Kwon, *Bull. Korean Chem. Soc.*, 2002, **23**, 933–934.
- 33 H. S. Kim, Y. H. Kim, S. K. Ahn and S. K. Kwon, *Macromolecules*, 2003, **36**, 2327–2332.
- 34 J. P. Hu, Y. F. Li, Z. Y. Ji, G. Y. Jiang, L. M. Yang, W. P. Hu, H. J. Gao, L. Jiang, Y. Q. Wen, Y. L. Song and D. B. Zhu, *J. Mater. Chem.*, 2007, **17**, 3530–3535.
- 35 J. Cornforth, R. H. Cornforth and R. T. Gray, *J. Chem. Soc., Perkin Trans. 1*, 1982, 2289–2296.
- 36 A. J. Campbell, D. D. C. Bradley and D. G. Lidzey, *J. Appl. Phys.*, 1997, **82**, 6326–6342.
- 37 (a) K. L. Jensen, *J. Vac. Sci. Technol., B*, 2003, **21**, 1528–1544; (b) L. Li, Q. D. Ling, S. L. Lim, Y. P. Tan, C. Zhu, D. S. H. Chan, E. T. Kang and K. G. Neoh, *Org. Electron.*, 2007, **8**, 401–406.
- 38 P. Mark and W. Helfrich, *J. Appl. Phys.*, 1962, **33**, 205–215.
- 39 (a) J. Frenkel, *Phys. Rev.*, 1938, **54**, 647–648; (b) C. Laurent, E. Kay and N. Souag, *J. Appl. Phys.*, 1998, **64**, 336–343.
- 40 Q. D. Ling, W. Wang, Y. Song, C. X. Zhu, D. S. H. Chan, E. T. Kang and K. G. Neoh, *J. Phys. Chem. B*, 2006, **110**, 23995–24001.
- 41 Y. Yonekuta, K. Honda and H. Nishide, *Polym. Adv. Technol.*, 2008, **19**, 281–284.
- 42 S. B. Heidenhain, Y. Sakamoto, T. Suzuki, A. Miura, H. Fujikawa, T. Mori, S. Tokito and Y. Taga, *J. Am. Chem. Soc.*, 2000, **122**, 10240–10241.
- 43 A. Facchetti, M. H. Yoon, C. L. Stern, H. E. Katz and T. J. Marks, *Angew. Chem., Int. Ed.*, 2003, **42**, 3900–3903.
- 44 A. Facchetti, M. Musherush, M.-H. Yoon, G. R. Hutchison, M. A. Ratner and T. J. Marks, *J. Am. Chem. Soc.*, 2004, **126**, 13859–13874.
- 45 K. Geramita, Y. Tao, R. A. Segalman and T. D. Tilley, *J. Org. Chem.*, 2010, **75**, 1871–1887.
- 46 F. Babudri, G. M. Farinola, F. Naso and R. Ragni, *Chem. Commun.*, 2007, 1003–1022.
- 47 I. Cacelli, A. Ferretti, M. Girlanda and M. Macucci, *Chem. Phys.*, 2006, **320**, 84–94.